

ANN prediction of impact toughness of ship steel/stainless steel plates produced by explosive welding

Yakup Kaya*, Ali Kalyon and Nizamettin Kahraman

Department of Manufacturing Engineering, Technology Faculty, Karabük University, Karabük 78050, Turkey

**Corresponding Author: ykaya@karabuk.edu.tr*

Submitted: 09/04/2018

Revised: 17/07/2019

Accepted: 21/10/2019

ABSTRACT

In this study, ship steel/stainless steel plates were produced by joining ship steel with stainless steel using explosive welding process. The characterization of the joining interface of the plates was carried out by optical microscopic examination. Charpy impact tests were conducted at different temperatures to determine the impact toughness of the ship steel/stainless steel plates and the effect of the rolling on the impact toughness. In addition, after the Charpy impact test, the fractured surfaces of the specimens were investigated via scanning electron microscopy (SEM). Using the data obtained as a result of the impact toughness tests, an artificial neural network (ANN) model was improved for the prediction of the impact toughness. Five different material types, two different rolling directions, and eight different temperatures were used as the input parameters of the Charpy impact tests. The impact toughness values obtained at the end of the tests were used as the output parameters of the generated prediction model. The high R^2 value obtained in the developed prediction model demonstrated that it could be successfully used for predicting impact toughness.

Keywords: ANN; explosive welding/cladding; impact toughness; ship steel plate; stainless steel.

INTRODUCTION

Today's ship and offshore construction designers face complex problems in selecting materials that provide minimization of topside weight and protection against marine corrosion-all within a reasonable budget (Kaya & Kahraman, 2013). With the development of modern industry, applications of single metallic constituents are unable to meet these requirements. Instead, with the respective merits of two metallic components, the clad plate can achieve the performance that single metal constituents fail to provide. The usual solution to this problem is to employ a variety of metals throughout the structure, each being selected for features appropriate for the specific component (Kaya, 2018).

A clad plate is a ship steel/stainless steel plate obtained by joining stainless steel (cladding metal), etc., to a carbon or low alloy steel (base metal). The most important advantage is that not only is it less costly than similar steels that are made entirely of cladding materials, but it also provides other features including good mechanical strength and good resistance to heat and corrosion. The explosive welding is utilized for many industrial processing applications, including those for refineries and chemical plants as well as in the ship-building industry. In the shipbuilding and marine industries, clad plates are one of the oldest applications for explosive welding (Kaya et al., 2017).

The explosive welding is becoming an increasingly popular process of joining, as it provides many advantages such as high joint strength and the ability to join unweldable metals or those difficult to weld by other processes. Additionally, when combining materials characterized by large surfaces or materials of different thicknesses, the explosive welding enables their properties to be preserved after joining (Fronczek et al., 2016).

New industrial application design requires the investigation of innovative construction materials, including multilayer materials such as bimetal. The explosive welding is one of the most widely employed processes for bimetal surface modification. This process offers the possibility of combining the properties of two or more metals or alloys (Nieslony et al., 2016). The explosive welding method has been successfully shown for varied similar steel/steel plate (Acarer et al., 2003) and Al/Al plate (Gülenç et al., 2016) and dissimilar aluminium/steel plate (Fındık, 2011, Corigliano et al., 2018; Corigliano et al., 2018; Kaya, 2018), titanium/steel plate (Xie et al., 2018), and inconel 625/Ti6Al4V plate (Topolski et al., 2016) materials.

Using mathematical models in experimental studies provides savings in both time and cost. Experimental studies can be modeled using many mathematical and experimental design processes (Benyounis & Olabi 2008). Previous studies have demonstrated the successful modeling of arc welding using artificial neural networks (ANNs) (Nagesh & Datta, 2002; Chan et al., 1999; Mirapeix et al., 2007). Moreover, other studies in the literature have used ANNs and other prediction models successfully to model the laser welding process (Casalino & Minutolo, 2004; Luo et al., 2005; Olabi et al., 2006), while a number of studies have obtained positive results using ANNs for other welding processes (Martin et al., 2007; Dutta & Prahitara, 2007; Shojaeefard et al., 2013).

Recently, a research has been carried out on the fatigue life (Prazmowski et al., 2017), numerical simulation (Chu et al., 2017), and physical/experimental modeling (Wang et al., 2016) of explosive-cladded plates. Reinforcement of these bimetallic composites with wire (Gülenç et al., 2016), their production from shape-memory alloys (Belyaev et al., 2016), and multilayer material production (Lazurenko et al., 2016) has also been studied. Much research has been carried out on the production and on the investigation of various aspects of explosive-cladded plates. However, the influences of distance from the explosion zone on the joining interface microstructure of these cladded plates have not been dealt with in those studies. Neither has any work been seen to deal with the impact transition temperature of these cladded plates nor to deal with the influence of the rolling direction of the base material on the impact transition temperature. In addition, no study found in the literature to date has employed ANNs to model the explosive welding.

Compared to the ship steels, the stainless steels provide much better mechanical and corrosion properties in sea water. Using entirely the stainless steel significantly increases the cost of shipbuilding. Instead, using the stainless steel on the surfaces exposed to corrosive effects (i.e., the outer surfaces) and normal shipbuilding steel on the less exposed surfaces may significantly decrease the cost. The aim of this study was to produce the ship steel/stainless steel plates for use in the offshore and shipbuilding industries by employing the explosive welding process to clad the ship steel plate widely used in shipbuilding with different types of the stainless steel (ferritic, austenitic, martensitic, and duplex). Based on the distance from the explosion zone, the effect of the rolling direction on the impact toughness of the resulting the ship steel/stainless steel plates was examined via microstructure studies. In addition, an ANN model was developed to evaluate the effect of the material type, the rolling direction, and temperature on the impact toughness.

MATERIAL AND METHODS

Material Production

For the ship steel/stainless steel plates production, the ship steel plates in dimensions of 500×250×10 mm were used as the base material and ferritic (AISI 430), austenitic (AISI 316L), martensitic (AISI 420), and duplex (AISI 2304). The stainless steel plates in dimensions of 500×250×1 mm were used as the cladding materials (flyer plate). The chemical compositions of the materials used in the ship steel/stainless steel plates are given in Table 1.

Table 1. Chemical compositions of the base and cladding materials (by weight %).

	C	Mn	P	S	Si	Al	Cu	Cr	Ni	Mo	Fe
Ship steel	0.149	0.70	0.015	0.012	0.166	0.028	0.049	0.022	0.052	0.002	Balance
AISI 430	0.039	0.340	0.029	0.002	0.39	-	-	16.07	0.15	-	Balance
AISI 316L	0.008	1.75	0.045	0.003	0.95	-	-	17.8	12	2.7	Balance
AISI 420	0.20	0.70	0.002	0.003	0.20	0.006	0.13	12.7	0.15	-	Balance
AISI 2304	0.02	0.10	-	-	-	-	-	23	4.8	0.3	Balance

The production of the ship steel/stainless steel plates using the explosive welding/cladding process was carried out using the parallel setup shown in Figure 1. Preliminary tests were conducted to determine the optimum welding parameters, which are given in Table 2. 92% ammonium nitrate, 5% diesel fuel, and min 3% TNT (Elbar-5) powder produced by Mechanical and Chemical Industry Company (MKE, Turkey) were used as the explosive in the welding processes. The specimens joined via the explosion could cool in the open air after the procedure.

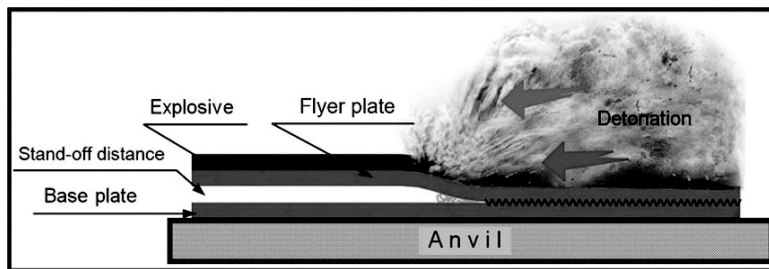


Fig. 1. Parallel arrangement of experimental setup for welding process.

Table 2. Welding parameters used in experimental studies.

Base Plate	Flyer Plate	Explosive Material	Stand-off Distance ((s) mm)	Explosive Rate (R)	Explosive Amount (m × R) (g)
Ship steel	AISI430	Elbar-5	2 t	2.5	2.500
	AISI316L				
	AISI420				
	AISI2304				

Metallographic Examination

The specimens were cut from the ship steel/stainless steel plates using the wire electric discharge machining (EDM) process for the microstructure examination and Charpy impact test. The microstructure specimens were classified according to their distance from the explosion zone (Zones 1-4) and the Charpy impact specimens were classified depending on the rolling direction (Fig. 2).

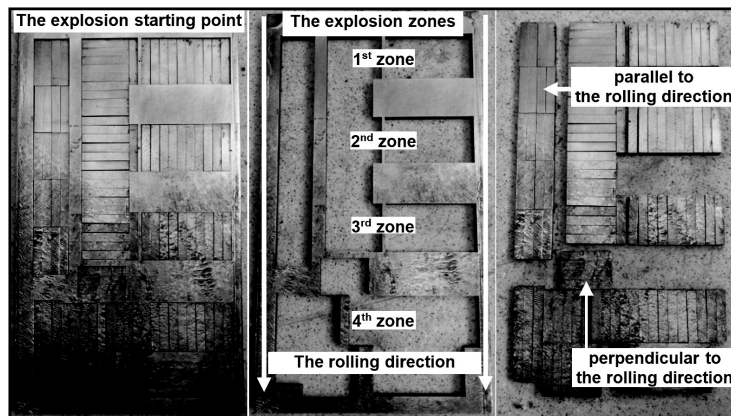


Fig. 2. Wire EDM-cut specimens.

The specimens for microstructure examinations were classified into four zones depending on the distance from the explosion zone and were cut, mounted in bakelite, and embedded in epoxy resin. Standard metallographic specimen preparation procedures (ground and polished) were then applied. The polished specimens were etched with 3% nitric acid-97% ethanol solution. Microstructure examinations were then performed using a Leica DM 4000M optical microscope.

Charpy Impact Toughness Tests

The base material (the ship steel plate) and the ship steel/stainless steel plates (four different cladding) were prepared in accordance with the Charpy impact test specimen standard (ASTM E 23-98) schematically shown in Figure 3. The specimens were cut from the plates in directions parallel and perpendicular to the rolling direction. In order to see the effect of the four different types of the stainless steel claddings (flyer plate) on the impact toughness of the ship steel base material, only the ship steel surface was notched. Tests were performed at eight different temperatures (between $-50\text{ }^{\circ}\text{C}$ and $50\text{ }^{\circ}\text{C}$) to determine the impact transition temperature of the specimens. Three specimens were tested at each temperature and the results averaged. The Charpy impact test specimens were brought to the test temperature using a HUBER CC 805 cooler/heater with a capacity of $-80\text{ }^{\circ}\text{C}/+150\text{ }^{\circ}\text{C}$. Charpy impact tests were applied to the prepared specimens using a computer-controlled 450 J capacity ZWICK ROELL RKP 450 device. After the tests, the fracture surface images ($-50\text{ }^{\circ}\text{C}$, $-40\text{ }^{\circ}\text{C}$, and $-30\text{ }^{\circ}\text{C}$) on the impact transition temperature of the ship steel and the ship steel/stainless steel plate specimens parallel to the rolling direction were examined with the ZEISS EVO LS10 scanning electron microscope (SEM).

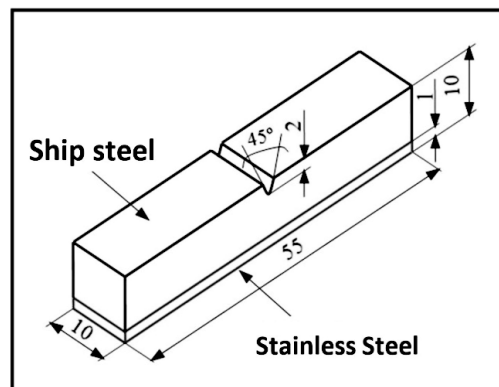


Fig. 3. Charpy impact test specimen.

Artificial Neural Networks

Artificial neural networks (ANNs) are computer systems that are developed with the aim of automatically performing a function resembling that of the human brain in its ability to derive, create, and discover new information on its own through the process of learning. An ANN is a processor whose structure is composed of simple process cells distributed in an intense parallelism having the ability to store and use information. This processor is like the brain as it uses connections between neurons, known as synaptic weights, to store knowledge and information that is learned through training (Balasubramanian et al., 2010).

In ANN models, the weight values necessary to increase the accuracy level of the outputs are firstly determined by using various transfer functions. In the training of an ANN, the weights are determined using the data in hand to reveal the relation between the input variables and the predicted variables. Once the ANN training is completed, the ANN may run and predictions may be produced (Manikya Kanti & Srinivasa Rao, 2008). The performance of a network is measured by its defined signal and error criterion. The output of the network is compared with the desired output to obtain the error margin. This process is repeated several times and the network is trained. The purpose of the training process is to achieve optimal solutions based on performance measures. Figure 4 shows the structure of an ANN.

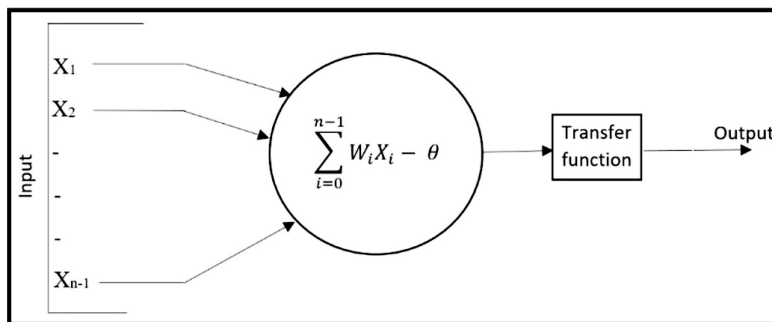


Fig. 4. Artificial neural network architecture (Palani & Natarajan, 2011).

An ANN is a parallel processor with the ability to collect information after a learning process and to store and generalize this information using connection weights between processing units. The process involves learning algorithms that enable the renewal of ANN weights to achieve the desired goal. It is defined as the generation of appropriate responses by ANN via generalization for entries that are not encountered in the training or learning process. With these superior features and as a result of the ability to solve complex problems, ANN applications are found in many engineering fields today (Mathew et al., 2017; Pouraliakbar et al., 2015; Palavar et al., 2015; Khorasani & Yazdi 2017; Almonacid et al., 2017).

RESULTS AND DISCUSSION

Metallographic Examination Results

Microstructure examinations were carried out to study the effect of the distance from the explosion zone on the structure of the joining interface of the ship steel/stainless steel plate specimens joined by the explosive welding. Images of the joining interface of the ship steel/stainless steel plates produced are shown in Figure 5.

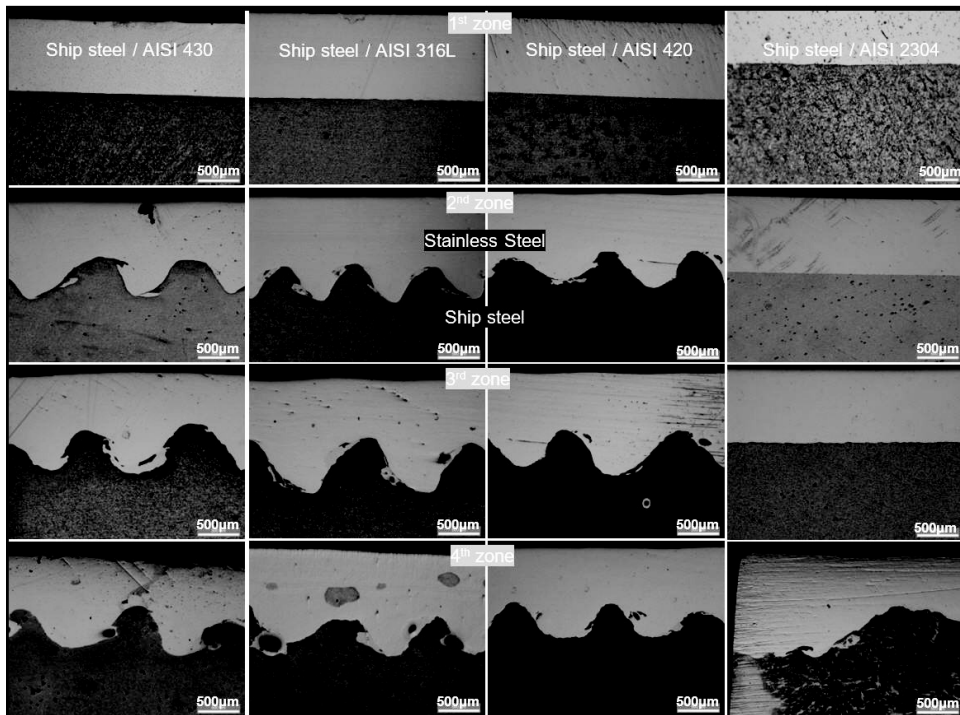


Fig. 5. The joining interface of the ship steel/stainless steel plates.

Figure 5 shows that the joining interface has a flat appearance in Zone 1, which was the nearest to the explosion zone. Moving away from the explosion zone (Zone 2), the waviness starts on the joining interface and the entire joining interface, excluding that of the ship steel/AISI 2304 plate, is wavy. Moving further away from the explosion zone (Zones 3 and 4), there is a noticeable increase in the length and amplitude of the waves on the joining interface. There was less waviness in the ship steel/AISI 2304 plate joining interfaces compared to those of the other plates, especially in Zones 2 and 3. Therefore, because the waviness in the joining interfaces varied depending on the amount of deformation, it was observed that the AISI 2304 was more rigid than the other cladding materials (AISI 430, AISI 316L, and AISI 420). In the literature (Kaya, 2014), it is reported that, in the explosive welding process, the wavy structure on the joining interface is related to the deformation and the waviness on the joining interface increases as the deformation amount increases. Moreover, they studied (Akbari Mousavi & Al-Hassani, 2005) the microstructures formed on the joining interface in the explosive welding process and observed that various structures (morphologies) on the joining interface (i.e., shear deformation and plastic strain) depended on the collision speed along the joining interfaces of the plates. At the same time, they reported that more shear deformation caused greater variation in the morphology of the joining interface. In other words, with low shear deformation, the joining interface was flat, while increasing shear deformation caused a wavy structure and with further shear deformation swirling waves were observed.

When the microstructure images of the joining interface of the ship steel/stainless steel plates were generally evaluated, the distance from the explosion zone, the waviness on the joining interface, and, accordingly, the length and amplitude of the waves were seen to increase. It was also determined that the amount of deformation increased as the distance from the explosion zone increased. In the literature, microstructure studies based on the distance from the explosion zone are extremely limited. They produced (Kaya et al., 2017) ship steel/AISI 2304 plate material via the explosive welding process and examined the effects of the distance from the explosion zone. They reported similar microstructure study results. Earlier studies (Miao et al., 2014; Durgutlu et al., 2005; Kahraman et al., 2005; Manikandan et al., 2006) have also found that collision speed and, consequently, collision pressure on the plates

increased due to the energy of the explosion on the joining interface of clad plates produced via the explosive welding using different explosive ratios. These studies also found that deformation increased with the increase of this pressure and the waviness increased in parallel with it. In addition, the effects shown by moving further from the explosion zone were like those shown by increasing the explosive ratio.

Charpy Impact Toughness Results

The Charpy impact test results of the ship steel plate and the ship steel/stainless steel plates at different temperatures in parallel to the rolling direction are shown in Figure 6 and perpendicular to the rolling direction in Figure 7.

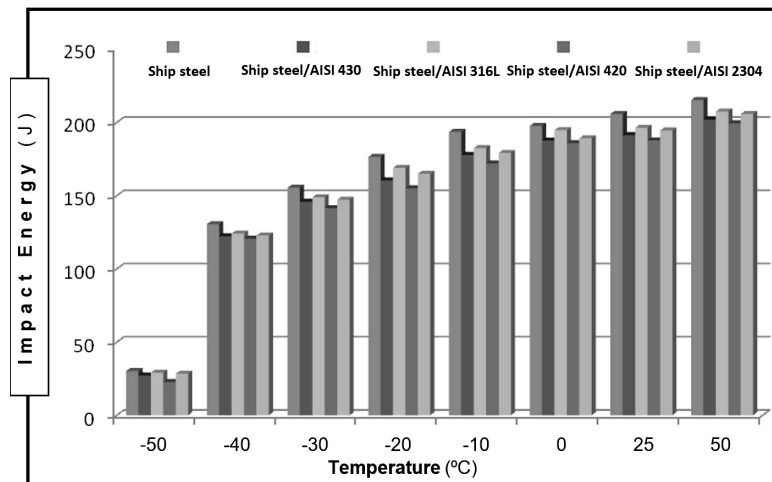


Fig. 6. Charpy impact test results of the ship steel/stainless steel plates in parallel to the rolling direction.

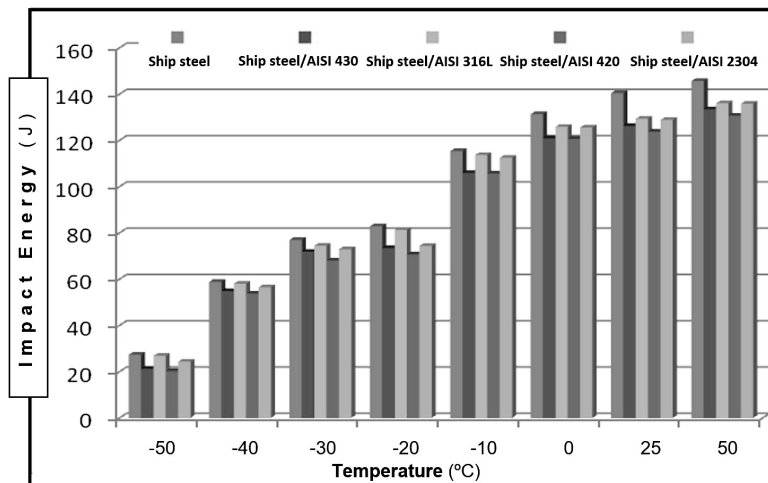


Fig. 7. Charpy impact test results of the ship steel/stainless steel plates perpendicular to the rolling direction.

When the Charpy impact test results of the specimens in parallel with and perpendicular to the rolling direction are examined, it can be seen that the lowest impact toughness was obtained from the ship steel/AISI 420 plate materials perpendicular to the rolling direction below -50 °C with 20.3 J, while the highest impact toughness was obtained from the ship steel base material in parallel to the rolling direction under 50 °C with 215.4 J. Furthermore, at all temperatures,

the specimens parallel to the rolling direction had higher impact toughness than the specimens perpendicular to the rolling direction. It has been reported in the literature (Kaya, 2014) that as plates were rolled, particles got longer in the direction of the rolling and, accordingly, V-Charpy specimens taken longitudinally (parallel to the rolling direction) exhibited higher impact toughness values compared to specimens taken horizontally (perpendicular to the rolling direction).

When Figures 6 and 7 are assessed together, it can be clearly seen that the impact toughness increased as the temperature increased in all specimens (the ship steel and the ship steel/stainless steel plates). In addition, the specimens parallel to the rolling direction showed impact transition temperatures between $-40\text{ }^{\circ}\text{C}$ and $-50\text{ }^{\circ}\text{C}$, while those perpendicular to the rolling direction showed impact transition temperatures between $-10\text{ }^{\circ}\text{C}$ and $-20\text{ }^{\circ}\text{C}$. There was almost no difference at low temperatures, although the difference in the impact toughness between specimens parallel and perpendicular to the rolling direction at high temperatures was high. They reported (Kaya et al., 2017) that, as a result of Charpy impact tests, specimens parallel to the rolling direction exhibited higher values of impact toughness than specimens perpendicular to the rolling direction and at the same time, specimens parallel to the rolling direction exhibited higher impact transition temperature values than perpendicular specimens. They also reported that the difference in toughness between different the rolling directions at high temperatures was high and the difference was low at low temperatures. They also reported that the ship steel/AISI 2304 plates exhibited lower impact toughness values compared to the ship steel due to the high deformation during the explosive welding.

As an example, Figure 8 shows images of the ship steel/AISI 430 plate specimens parallel and perpendicular to the rolling direction after the Charpy impact test at all test temperatures.

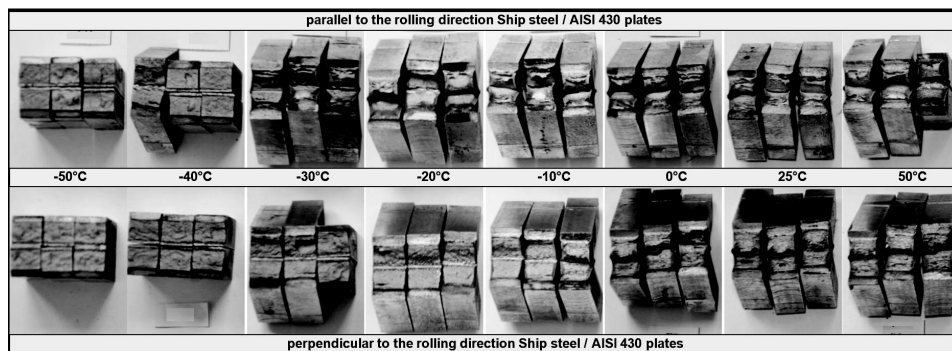


Fig. 8. The ship steel/AISI 430 plate specimens after Charpy impact test.

Examination of the specimen images in Figure 8 shows that the specimens below the impact transition temperature ($-40\text{ }^{\circ}\text{C}$ for the ship steel and the ship steel/stainless steel plates parallel to the rolling direction and $-10\text{ }^{\circ}\text{C}$ for the ship steel and the ship steel/stainless steel plates perpendicular to the rolling direction) displayed a brittle fracture type and the fracture is flat without plastic deformation. It can also be observed that the fracture surfaces had a fine-grained and shiny appearance. The specimens exceeding the impact transition temperature showed a ductile fracture type, having first undergone a plastic shape change before fracturing. In addition, the fractures were in the form of tears with surfaces exhibiting a fibrous appearance. The literature reports (Kaya et al., 2017) that the explosive welding process was used to produce ship steel/AISI 2304 plate materials to produce ship steel/AISI 316L plate (Kaya & Kahraman, 2013), to produce P355GH/AISI 316L plate (Kaçar & Acarer, 2004), and to produce P355GH/AISI 2205 plate (Kaçar & Acarer, 2003). They all reported similar results following Charpy impact tests at different temperatures.

Fracture Surface SEM Studies

The fracture surfaces of the ship steel and the ship steel/stainless steel plates parallel to the rolling direction and exceeding impact transition temperatures ($-50\text{ }^{\circ}\text{C}$, $-40\text{ }^{\circ}\text{C}$, and $-30\text{ }^{\circ}\text{C}$) were examined by SEM. Images of the fractured surfaces are shown in Figure 9.

The fractured surface SEM images show that the specimens parallel to the rolling direction at -50 °C were flat and cut through the grain. In addition, these fracture surfaces appeared to be brittle, reflecting light and having a shiny appearance. The specimens parallel to the rolling direction at -40 °C and -30 °C had a tear-like surface image, including microspaces joined due to plastic deformation, with protrusions and fibrous appearance. They produced (Kaçar & Acarer, 2004) P355GH/AISI 316L plates using the explosive welding. Charpy impact tests at different temperatures were applied, and SEM studies were performed on the fractured surfaces after the Charpy impact test. They reported that a predominant ductile fracture surface was obtained at 25 °C characterized by a growth of micro voids and intramolecular fractures, while cracking and a fracture-like appearance through the grain were obtained at -50 °C.

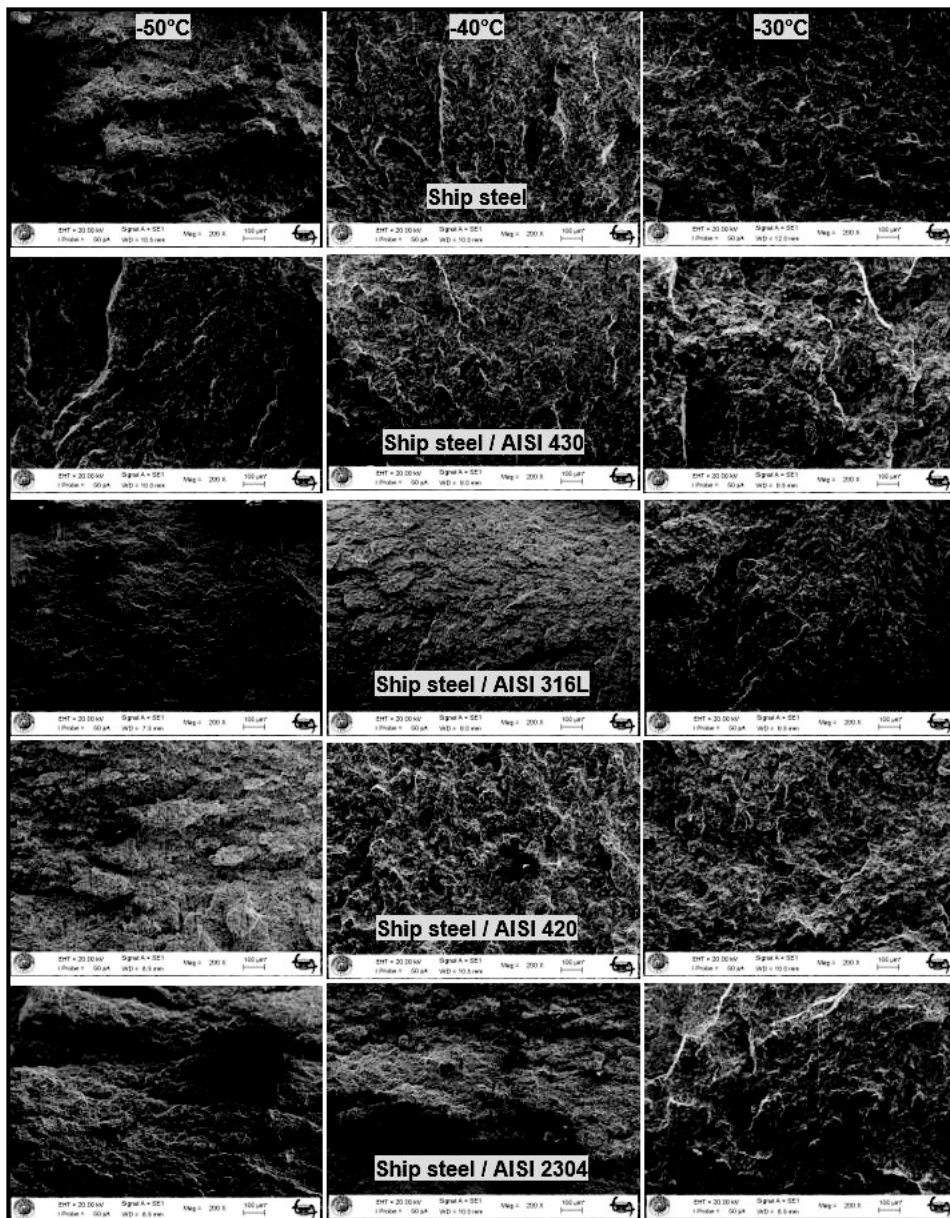


Fig. 9. SEM images of fractured surfaces of the ship steel/stainless steel plates.

In addition, using the explosive welding process, they produced the ship steel/AISI 2304 (Kaya et al., 2017) and P355GH/AISI 2205 (Kaçar & Acarer 2003) plates. They applied Charpy impact tests at different temperatures and then performed SEM studies on the surfaces of the fractured specimens and reported similar results above and below the impact transition temperature.

ANN Application

Artificial neural networks are an estimation model that is created by using the data contained in the experimental set. The learning of the ANN model is performed by using the values in the experiment set. After learning is performed, the model is tested. The more the inputs used in learning the model, the more successful the model. The purpose of testing the model is to evaluate the predictability of the model. When testing the ANN model, experimental parameters that are not used in learning the model are used. Prediction and evaluation results are compared to determine whether the model is successful. Experimental results can be estimated without the need for an experimental set using the ANN model, which has been successfully created. This saves time and costs for experimental work. Using the ANN model, which is obtained with high estimation results, it is provided to estimate the impact toughness results for the material under the desired properties and conditions. The fact that the model can only work in the range of data used in learning causes the system to work in a limited way.

In this study, the Levenberg-Marquardt (LM) algorithm based on a backpropagation multilayered ANN model was used due to its widespread usage and application in ANNs. The LM learning algorithm is a very successful optimization process and backpropagation learning technique based on the idea of multiple neighborhoods and the least squares approach. One of the most important advantages of the LM algorithm is its fast convergence. The prediction performance of the ANN model developed in this experimental study was established by applying the determination coefficient (R^2), root of mean square error (RMSE), and mean absolute percentage error (MAPE) processes. Equations (1), (2), and (3) below were used in the calculations.

$$R^2 = 1 - \left[\frac{\sum(\Delta IT_{experiment} - \Delta IT_{ANN})^2}{\sum(\Delta IT_{ANN})^2} \right] \quad (1)$$

$$RMSE = \left[\frac{1}{n} \sum_{i=1}^n (IT_{ANN} - \Delta IT_{experiment})^2 \right]^{\frac{1}{2}} \quad (2)$$

$$MAPE = \frac{\Delta IT_{ANN} - \Delta IT_{experiment}}{\Delta IT_{ANN}} \times 100 \quad (3)$$

Pythia software was used to develop the ANN model. Training was given by using the Fermi function as the Pythia software transfer function. The Fermi transfer function can be calculated by Equation (4), where V_N represents the normalization value of the input, and w_i represents the weight value and ($i = 1, 2, 3 \dots, n$).

$$F_i = \frac{1}{1 + e^{-4(\sum V_N \times w_i - 0.5)}} \quad (4)$$

The training and testing experiments for the modeling of the impact strength results by the ANN were first determined. Subsequently, for each of the 80 experiments conducted according to temperature, material type, and the rolling direction, 68 pieces of experimental data to be used for training and 12 pieces for testing purposes were randomly separated. The most appropriate network structures and number of neurons were investigated by training the ANN with the experimental results. Firstly, a network structure having the lowest deviation value was chosen by automatic optimization of the program. After the network structure was determined, by changing the number of cycles and learning ratios of the program, it was trained to the lowest deviation value. For the experiments conducted as the result of these processes, a network structure consisting of four layers and 16 neurons was chosen. The network structure obtained is shown in Figure 10.

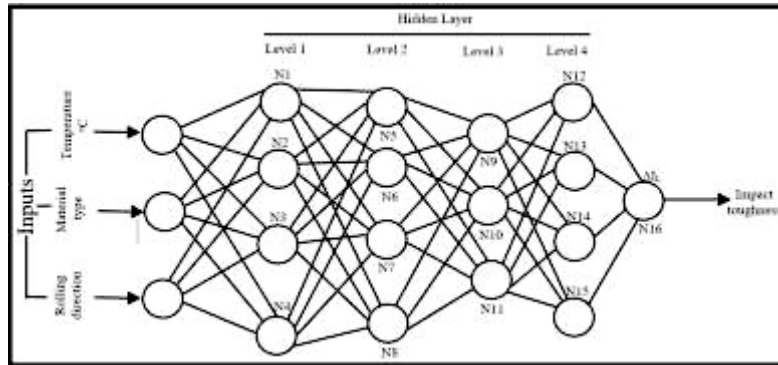


Fig. 10. Network structure.

The five different material types, which were the input parameters of the ANN, were classified from 1 to 5 and numerical responses to the material types were determined. The ship steel was designated as 1 and the others were numbered sequentially. Parallel to the rolling direction was designated as 1, and 2 was assigned for perpendicular to the rolling direction. Table 3 shows the 68 pieces of data used in training the network.

Table 3. Experimental results and ANN learning outcomes.

Sq.	Material type	Rolling direction	Temperature (°C)	Impact toughness (J) (Experimental results)	Impact toughness (J) (ANN-predicted)
1	Ship steel	Parallel	-50	30.3	31.206
2	Ship steel	Parallel	-30	155.5	157.475
3	Ship steel	Parallel	-20	176.5	175.743
4	Ship steel	Parallel	-10	193.6	189.395
5	Ship steel	Parallel	0	197.7	198.068
6	Ship steel	Parallel	25	205.9	205.794
7	Ship steel	Parallel	50	215.4	206.976
8	Ship steel	Perpendicular	-50	27.4	22.792
9	Ship steel	Perpendicular	-40	58.9	54.484
10	Ship steel	Perpendicular	-30	77	71.770
11	Ship steel	Perpendicular	-20	82.9	78.056
12	Ship steel	Perpendicular	0	131.4	125.295
13	Ship steel	Perpendicular	50	145.7	138.588
14	Ship steel/AISI 430	Parallel	-50	27.3	25.976
15	Ship steel/AISI 430	Parallel	-40	122.4	120.981
16	Ship steel/AISI 430	Parallel	-20	160.5	163.431
17	Ship steel/AISI 430	Parallel	-10	177.9	178.816
18	Ship steel/AISI 430	Parallel	0	187.7	190.082
19	Ship steel/AISI 430	Parallel	25	191.4	201.489
20	Ship steel/AISI 430	Parallel	50	202	203.670
21	Ship steel/AISI 430	Perpendicular	-40	54.9	56.754
22	Ship steel/AISI 430	Perpendicular	-30	71.9	71.794
23	Ship steel/AISI 430	Perpendicular	-20	73.5	78.169
24	Ship steel/AISI 430	Perpendicular	-10	106	110.286

25	Ship steel/AISI 430	Perpendicular	0	120.9	124.273
26	Ship steel/AISI 430	Perpendicular	25	126.3	133.204
27	Ship steel/AISI 316L	Parallel	-50	29.2	25.592
28	Ship steel/AISI 316L	Parallel	-40	124.2	120.767
29	Ship steel/AISI 316L	Parallel	-30	149	144.356
30	Ship steel/AISI 316L	Parallel	-20	169	161.367
31	Ship steel/AISI 316L	Parallel	-10	182.6	176.571
32	Ship steel/AISI 316L	Parallel	0	194.8	187.812
33	Ship steel/AISI 316L	Parallel	50	207.6	202.015
34	Ship steel/AISI 316L	Perpendicular	-50	26.9	24.870
35	Ship steel/AISI 316L	Perpendicular	-40	58.1	58.460
36	Ship steel/AISI 316L	Perpendicular	-30	74.5	71.811
37	Ship steel/AISI 316L	Perpendicular	-20	81.3	78.242
38	Ship steel/AISI 316L	Perpendicular	-10	113.7	110.044
39	Ship steel/AISI 316L	Perpendicular	0	125.9	123.333
40	Ship steel/AISI 316L	Perpendicular	25	129.4	131.849
41	Ship steel/AISI 420	Parallel	-50	22.8	26.267
42	Ship steel/AISI 420	Parallel	-40	120.6	123.623
43	Ship steel/AISI 420	Parallel	-30	141.5	146.448
44	Ship steel/AISI 420	Parallel	-20	155.1	163.341
45	Ship steel/AISI 420	Parallel	-10	172.1	178.005
46	Ship steel/AISI 420	Parallel	25	187.8	199.045
47	Ship steel/AISI 420	Parallel	50	199.5	201.401
48	Ship steel/AISI 420	Perpendicular	-50	20.3	25.757
49	Ship steel/AISI 420	Perpendicular	-40	53.8	59.225
50	Ship steel/AISI 420	Perpendicular	-30	68.1	71.818
51	Ship steel/AISI 420	Perpendicular	-20	70.7	78.423
52	Ship steel/AISI 420	Perpendicular	0	120.7	122.813
53	Ship steel/AISI 420	Perpendicular	25	123.8	130.939
54	Ship steel/AISI 420	Perpendicular	50	130.7	135.176
55	Ship steel/AISI 2304	Parallel	-50	28.5	27.686
56	Ship steel/AISI 2304	Parallel	-40	122.9	127.486
57	Ship steel/AISI 2304	Parallel	-30	147.3	149.782
58	Ship steel/AISI 2304	Parallel	-10	179.2	180.512
59	Ship steel/AISI 2304	Parallel	0	189.3	189.815
60	Ship steel/AISI 2304	Parallel	25	194.6	199.100
61	Ship steel/AISI 2304	Parallel	50	205.9	201.210
62	Ship steel/AISI 2304	Perpendicular	-50	24.4	27.686
63	Ship steel/AISI 2304	Perpendicular	-40	56.5	58.006
64	Ship steel/AISI 2304	Perpendicular	-20	74.4	79.132
65	Ship steel/AISI 2304	Perpendicular	-10	112.5	111.687
66	Ship steel/AISI 2304	Perpendicular	0	125.6	123.468
67	Ship steel/AISI 2304	Perpendicular	25	128.9	131.210
68	Ship steel/AISI 2304	Perpendicular	50	135.9	135.883

In the training of an ANN, the process is slowed down by the application of a raw dataset. Thus, for more efficient and faster training, normalization preprocessing was applied to the data provided to the ANN. In this study, the data used in the ANN were normalized using the min-max process, which linearly normalizes the data. The minimum is the lowest possible data value, while the maximum is the highest possible data value. Equation (5) was used to reduce the data in Table 4 to values of between 0 and 1 using the min-max process. The weight values of the ANN are given in Tables 5, 6, 7, and 8, respectively.

$$V_N = \frac{V_R - V_{min}}{V_{max} - V_{min}} \tag{5}$$

In this equation,

V_N = normalized data,

V_R = input value,

V_{min} = the smallest number within the input set,

V_{max} = the largest number within the input set.

Table 4. Normalization values.

	V_{min}	V_{max}
Material type (V_{MT})	1	5
Rolling direction (V_{RD})	1	2
Temperature (°C) (V_T)	-50	50
Impact toughness (J) (V_{IT})	20.3	215.4

Table 5. Weights of neurons in Level-1.

	N1	N2	N3	N4
W_1	0.0506250	0.2191430	0.1748540	-1.0362710
W_2	1.0109940	0.5882470	0.2676310	2.3628070
W_3	-3.3954180	-0.4252060	1.4197170	-0.1938420

Table 6. Weights of neurons in Level-2.

	N5	N6	N7	N8
W_1	3.5515710	-1.0981070	-1.4290500	-0.7202270
W_2	0.4571720	-0.0847450	0.6644960	0.2412670
W_3	-1.4280560	-0.7568220	-0.0040730	0.6043190
W_4	0.8750400	0.4520700	1.0166050	2.2039020

Table 7. Weights of neurons in Level-3.

	N9	N10	N11
W_1	-1.3203310	-0.3198730	2.2103570
W_2	0.4644580	-0.5137680	-0.4650200
W_3	-1.0242260	0.3772490	-2.3448160
W_4	1.1273880	-0.8481280	-1.4287730

Table 8. Weights of neurons in Level-4 and output.

	N12	N13	N14	N15	Output
W₁	-1.0730750	0.3549820	-1.5653750	0.5261540	-0.594484
W₂	0.6896290	-0.6594090	-0.2935870	1.2950210	1.489708
W₃	0.9386280	-0.7053140	1.1983560	-1.4338800	-1.447591
W₄					2.547669

The performance of the ANN was evaluated by using the R², the RMSE, and the MAPE specified in Equations (1), (2), and (3). High R² and low RMSE values indicated that the prediction model was successful.

The ANN created was constructed using sixteen neurons, feedforward, and the backpropagation algorithm. The model was formulated using the widely applied Fermi transfer function in ANN training (Eq. 4). At the end of the calculations, the net output value was calculated using Equation (6).

$$V_{ann} = f_i (V_{max} - V_{min}) + V_{min} \tag{6}$$

where f_i ($i = 1, 2, 3, \dots, n$), V_{max} is the maximum output value of the experimental data, and V_{min} is the minimum output value.

Once the learning part of the network was successfully completed, the network performance was tested using the experimental data not used in the learning. The output of the fifteen-neuron network structure generated for the prediction of impact toughness is given in Equations (7-11). These equations were used to calculate the impact toughness value by using material type, the rolling direction, and temperature input values.

$$F_i = \frac{1}{1 + e^{-4(\sum V_{MT} \cdot W_{1i} + V_{RD} \cdot W_{2i} + V_T \cdot W_{3i} - 0.5)}} \tag{7}$$

$$G_i = \frac{1}{1 + e^{-4(\sum F_1 \cdot W_{1i} + F_2 \cdot W_{2i} + F_3 \cdot W_{3i} + F_4 \cdot W_{4i} - 0.5)}} \tag{8}$$

$$H_i = \frac{1}{1 + e^{-4(\sum G_5 \cdot W_{1i} + G_6 \cdot W_{2i} + G_7 \cdot W_{3i} + G_8 \cdot W_{4i} - 0.5)}} \tag{9}$$

$$I_i = \frac{1}{1 + e^{-4(\sum H_9 \cdot W_{1i} + H_{10} \cdot W_{2i} + H_{11} \cdot W_{3i} - 0.5)}} \tag{10}$$

$$L_{\Delta IT} = \frac{1}{1 + e^{-4(\sum I_{12} \cdot W_{1i} + I_{13} \cdot W_{2i} + I_{14} \cdot W_{3i} + I_{15} \cdot W_{4i} + I_{16} \cdot W_{5i} - 0.5)}} \tag{11}$$

A comparison of the data obtained in the experimental studies and the impact toughness prediction values obtained by using the ANN prediction model is given in Figure 11. The ANN and the experimental results were very close to each other. Table 9 gives the R², RMSE, and MAPE results of the ANN learning prediction results. The ANN learning model R² value was 0.9941, the RMSE value was 4.4920, and the MAPE value was 4.2965. The high R² value and the low RMSE and MAPE values obtained indicated that the learning of the prediction model was successful.

Table 9. Statistical data of ANN model learning established for impact toughness prediction.

	R ²	RMSE	MAPE
Δ IT	0.9941	4.4920	4.2965

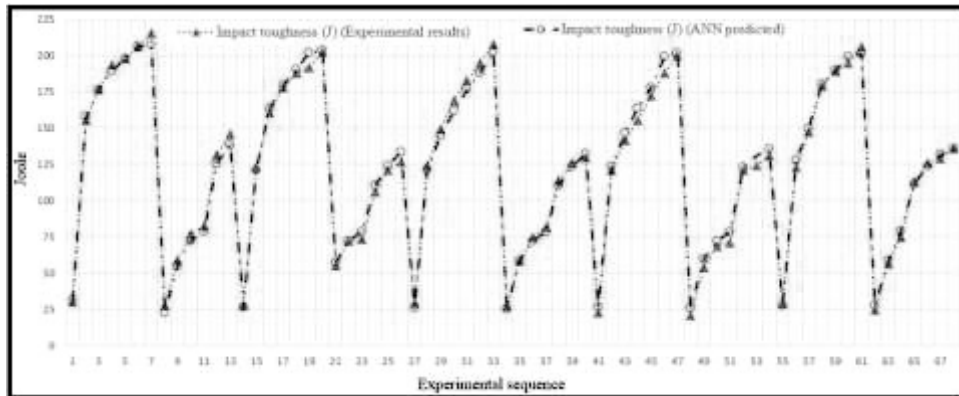


Fig. 11. Comparison of experimental results and ANN learning prediction results.

ANN Testing Results

The 68 experimental pieces of data shown in Table 3 were used for the learning of the network. The 12 randomly selected pieces of data given in Table 10 (which were not used for the learning of the network) were used in the testing of the network.

As shown in Figure 12, the experimental results and the ANN test results were close to each other. The values of the ANN test prediction model were 0.9954, 3.1458, and 2.7796 for R^2 , RMSE, and MAPE, respectively. The statistical results shown in Table 11 show that the established ANN model can be used successfully for prediction of impact toughness.

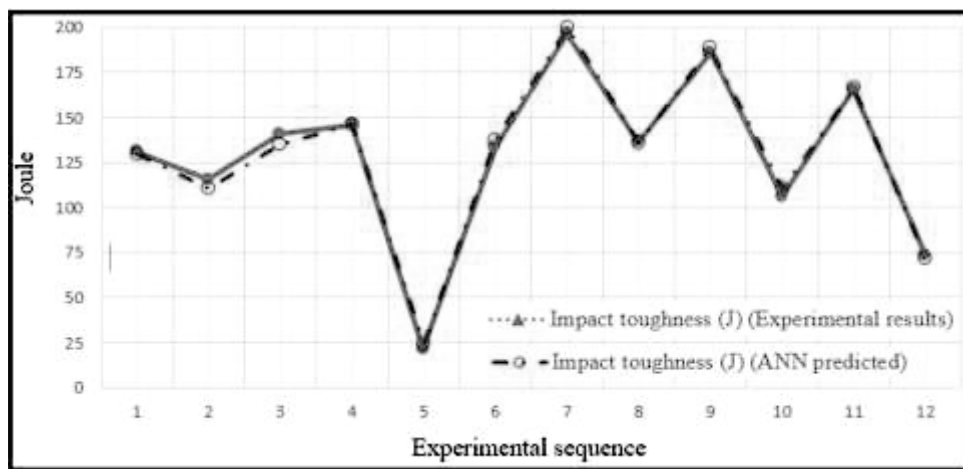
Table 10. Experimental results and ANN test outcomes.

Sq.	Material type	Rolling direction	Temperature (°C)	Impact toughness (J) (Experimental results)	Impact toughness (J) (ANN-predicted)
1	Ship steel	Parallel	-40	130.6	129.739
2	Ship steel	Perpendicular	-10	115.4	110.468
3	Ship steel	Perpendicular	25	140.5	134.692
4	Ship steel/AISI 430	Parallel	-30	145.9	145.853
5	Ship steel/AISI 430	Perpendicular	-50	21.3	23.761
6	Ship steel/AISI 430	Perpendicular	50	133.5	137.192
7	Ship steel/AISI 316L	Parallel	25	196.4	199.531
8	Ship steel/AISI 316L	Perpendicular	50	136.1	135.927
9	Ship steel/AISI 420	Parallel	0	185.9	188.399
10	Ship steel/AISI 420	Perpendicular	-10	105.7	110.182
11	Ship steel/AISI 2304	Parallel	-20	165	166.635
12	Ship steel/AISI 2304	Perpendicular	-30	73	71.804

Table 11. Test statistical data of ANN model established for impact toughness prediction.

	R^2	RMSE	MAPE
ΔIT	0.9954	3.1458	2.7796

The created ANN was able to calculate impact toughness values for different material types, different rolling directions, and different temperatures. A total of 80 experimental pieces of data were used, including 68 for training the ANN and 12 for testing the network. In order to evaluate the performance of the generated ANN, the values of the R^2 , the RMSE, and the MAPE were calculated. The high R^2 and low RMSE and MAPE values indicated that the ANN model generated could be used successfully in predicting impact toughness for different materials, different rolling directions, and different temperatures.

**Fig. 12.** Comparison of experimental results and ANN test prediction results.

CONCLUSIONS

In this study, microstructure, impact toughness, and fractured surface SEM studies were carried out on the ship steel/stainless steel plates produced through the explosive welding process. In addition, an ANN model was generated for the prediction of the impact toughness of these plates. The subsequent conclusions can be drawn from this present study:

- In the optical microscopic studies of the joining interface of the ship steel/stainless steel plate specimens, a flat joining interface was obtained near the explosion zone, while the distance from the explosion zone increased, and the joining interface transformed into the wavy structure. Furthermore, as the distance from the explosion zone increased, the wavelength and amplitude increased with increasing amount of cold deformation.
- As a result of the Charpy impact tests applied at different temperatures, specimens parallel to the rolling direction exhibited higher impact toughness values compared to specimens perpendicular to the rolling direction. Furthermore, the impact transition temperatures of the specimens parallel to the rolling direction were lower compared to those of the specimens perpendicular to the rolling direction.
- In the fractured surface SEM investigations, ductile fracture surfaces were seen at temperatures below the impact transition temperature and brittle fracture surfaces were found at temperatures above the impact transition temperature.
- The values obtained with the prediction model established by the ANN were very close to the experimental values. Statistical results showed that the prediction model was successful.

- By using a prediction model in experimental work, less time would be spent, and costs reduced. The desired data could be obtained without the need for an experimental environment. Moreover, the generated prediction model would provide a quick solution without the need to decide on experimental working conditions.

ACKNOWLEDGMENT

The authors are pleased to acknowledge the financial support for this study from Karabük University scientific research projects department (KBÜ-BAP-13/1-DR-012). We would also like to thank to Mechanical and Chemical Industry Company (MKE, Turkey) for the facilities they provide.

REFERENCES

- Acarer, M., Gülenç, B. & Fındık, F. 2003.** Investigation of explosive welding parameters and their effects on microhardness and shear strength. *Materials & Design* **24**:659-664. [https://doi.org/10.1016/S0261-3069\(03\)00066-9](https://doi.org/10.1016/S0261-3069(03)00066-9)
- Akbari, Mousavi, A.A. & Al-Hassani, S.T.S. 2005.** Numerical and experimental studies of the mechanism of the wavy interface formations in explosive/impact welding. *Journal of the Mechanis and Physics of Solids* **53**:2501-2528. <https://doi.org/10.1016/j.jmps.2005.06.001>
- Almonacid, F., Fernandez, E.F., Mellit, A. & Kalogirou, S. 2017.** Review of techniques based on artificial neural networks for the electrical characterization of concentrator photovoltaic technology. *Renewable & Sustainable Energy Reviews* **75**:938-953. <https://doi.org/10.1016/j.rser.2016.11.075>
- Balasubramanian, K.R., Buvanashakaran, G. & Sankaranarayanan, K. 2010.** Modeling of laser beam welding of stainless steel sheet butt joint using neural networks, *CIRP Journal of Manufacturing Science and Technology* **3**:80-84. <https://doi.org/10.1016/j.cirpj.2010.07.001>
- Belyaev, S., Rubanik, V., Resnina, N., Rubanik, Jr. V., Demidova, E. & Lomakin, I. 2016.** Bimetallic shape memory alloy composites produced by explosion welding: Structure and martensitic transformation. *Journal of Materials Processing Technology* **234**:323-331. <https://doi.org/10.1016/j.jmatprotec.2016.04.004>
- Benyounis, K.Y. & Olabi, A.G. 2008.** Optimization of different welding processes using statistical and numerical approaches—A reference guide. *Advances in Engineering Software* **39**:483-496. <https://doi.org/10.1016/j.advengsoft.2007.03.012>
- Casalino, G. & Minutolo, F.M.C. 2004.** A model for evaluation of laser welding efficiency and quality using an artificial neural network and fuzzy logic. *Proceedings of the Institution of Mechanical Engineers, Part B: Journal of Engineering Manufacture* **218**:641-646. <https://doi.org/10.1243/0954405041167112>
- Chan, B., Pacey, J. & Bibby, M. 1999.** Modelling gas metal arc weld geometry using artificial neural network technology. *Canadian Metallurgical Quarterly* **38**: 43-51. [https://doi.org/10.1016/S0008-4433\(98\)00037-8](https://doi.org/10.1016/S0008-4433(98)00037-8)
- Chu, Q., Zhang, M., Li, J. & Yan, C. 2017.** Experimental and numerical investigation of microstructure and mechanical behavior of titanium/steel interfaces prepared by explosive welding. *Materials Science and Engineering: A* **689**:323-331. <https://doi.org/10.1016/j.msea.2017.02.075>
- Corigliano, P., Crupi, V., Guglielmino, E. & Sili, A.M. 2018.** Full-field analysis of Al/Fe explosive welded joints for shipbuilding applications. *Marine Structures* **57**:207-218. <https://doi.org/10.1016/j.marstruc.2017.10.004>
- Corigliano, P., Crupi, V. & Guglielmino, E. 2018.** Non linear finite element simulation of explosive welded joints of dissimilar metals for shipbuilding applications. *Ocean Engineering* **160**:346-353. <https://doi.org/10.1016/j.oceaneng.2018.04.070>
- Durgutlu, A., Gülenç, B. & Fındık, F. 2005.** Examination of copper/stainless steel joints formed by explosive welding. *Materials & Design* **26**:497-507. <https://doi.org/10.1016/j.matdes.2004.07.021>
- Dutta, P. & Pratihar, D. K. 2007.** Modeling of TIG welding process using conventional regression analysis and neural network-based approaches. *Journal of Materials Processing Technology* **184**:56-68. <https://doi.org/10.1016/j.jmatprotec.2006.11.004>
- Fındık, F. 2011.** Recent developments in explosive welding. *Materials & Design* **32**(3):1081-1093. <https://doi.org/10.1016/j.matdes.2010.10.017>
- Fronczek, D.M., Wojewoda-Budka, J., Chulist, R., Sypien, A., Korneva A., Szulc, Z., Schell, N. & Zieba, P. 2016.** Structural

properties of Ti/Al clads manufactured by explosive welding and annealing. *Materials & Design* **91**:80-89. <https://doi.org/10.1016/j.matdes.2015.11.087>

- Gülenç, B., Kaya, Y., Durgutlu, A., Gülenç, İ.T., Yıldırım, M.S. & Kahraman, N. 2016.** Production of wire reinforced composite materials through explosive welding. *Archives Civil Mechanical Engineering* **16**:1-8. <https://doi.org/10.1016/j.acme.2015.09.006>
- Kaçar, R. & Acarer, M. 2003.** Microstructure-property relationship in explosively welded duplex stainless steel-steel, *Materials Science and Engineering: A* **363**:290-296. [https://doi.org/10.1016/S0921-5093\(03\)00643-9](https://doi.org/10.1016/S0921-5093(03)00643-9)
- Kaçar, R. & Acarer, M. 2004.** An investigation on the explosive cladding of 316L stainless steel-DIN-P355GH steel. *Journal of Materials Processing Technology* **52**:91-96. <https://doi.org/10.1016/j.jmatprotec.2004.03.012>
- Kahraman, N., Gülenç, B. & Fındık, F. 2005.** Joining of titanium/stainless steel by explosive welding and effect on interface. *Journal of Materials Processing Technology* **169**:127-133. <https://doi.org/10.1016/j.jmatprotec.2005.06.045>
- Kaya, Y. 2014.** An investigation into the microstructure, mechanical and corrosion properties of Grade A ship steel-stainless steel composites produced by explosive welding method. Ph D Thesis Karabük University.
- Kaya, Y. 2018.** Microstructural, mechanical and corrosion investigations of ship steel-aluminum bimetal composites produced by explosive welding. *Metals* **8**(7):544. <https://doi.org/10.3390/met8070544>
- Kaya, Y. & Kahraman, N. 2013.** An investigation into the explosive welding/cladding of Grade A ship steel/AISI 316L austenitic stainless steel. *Materials & Design* **52**:367-372. <https://doi.org/10.1016/j.matdes.2013.05.033>
- Kaya, Y., Kahraman, N., Durgutlu, A. & Gülenç, B. 2017.** Investigation of the microstructural, mechanical and corrosion properties of Grade A ship steel-duplex stainless steel composites produced via explosive welding. *Metallurgical and Materials Transactions A* **48**(8):3721-3733. <https://doi.org/10.1007/s11661-017-4161-3>
- Khorasani, A. & Yazdi, M.R.S. 2017.** Development of a dynamic surface roughness monitoring system based on artificial neural networks (ANN) in milling operation. *The International Journal of Advanced Manufacturing Technology* **93**(1-4):141-151. <https://doi.org/10.1007/s00170-015-7922-4>
- Lazurenko, D.V., Bataev, I.A., Mali, V.I., Bataev, A.A., Maliutina, I.N., Lozhkin, V.S., Esikov, M.A. & Jorge A.M.J. 2016.** Explosively welded multilayer Ti-Al composites: Structure and transformation during heat treatment. *Materials & Design* **102**:122-130.
- Luo, H., Zeng, H., Hu, L., Hu, X. & Zhou, Z. 2005.** Application of artificial neural network in laser welding defect diagnosis. *Journal of Materials Processing Technology* **170**:403-411. <https://doi.org/10.1016/j.jmatprotec.2005.06.008>
- Manikandan, P., Hokamoto, K., Deribaş, A.A., Raghukandan, K. & Tomoshige, R. 2006.** Explosive welding of titanium/stainless steel by controlling energetic conditions. *Materials Transactions* **47**(8):2049-2055. <https://doi.org/10.2320/matertrans.47.2049>
- Manikya, Kanti, K. & Srinivasa, Rao, P. 2008.** Prediction of bead geometry in pulsed GMA welding using back propagation neural network. *Journal of Materials Processing Technology* **200**:300-305. <https://doi.org/10.1016/j.jmatprotec.2007.09.034>
- Martín, O., López, M. & Martín, F. 2007.** Artificial neural networks for quality control by ultrasonic testing in resistance spot welding. *Journal of Materials Processing Technology* **183**:226-233. <https://doi.org/10.1016/j.jmatprotec.2006.10.011>
- Mathew, J., Moat, R.J., Paddea, S., Fitzpatrick, M.E. & Bouchard, P.J. 2017.** Prediction of residual stresses in girth welded pipes using an artificial neural network approach. *International Journal of Pressure Vessels and Piping* **150**:89-95. <https://doi.org/10.1016/j.ijpvp.2017.01.002>
- Miao, G., Ma, H., Shen, Z. & Yu, Y. 2014.** Research on honeycomb structure explosives and double sided explosive cladding. *Materials & Design* **63**:538-543. <https://doi.org/10.1016/j.matdes.2014.06.050>
- Mirapeix, J., García-Allende, P.B., Cobo, A., Conde, O.M. & López-Higuera, J.M. 2007.** Real-time arc-welding defect detection and classification with principal component analysis and artificial neural networks. *NDT & E International* **40**:315-323. <https://doi.org/10.1016/j.ndteint.2006.12.001>
- Nagesh, D.S. & Datta, G.L. 2002.** Prediction of weld bead geometry and penetration in shielded metal-arc welding using artificial neural networks. *Journal of Materials Processing Technology* **123**:303-312. [https://doi.org/10.1016/S0924-0136\(02\)00101-2](https://doi.org/10.1016/S0924-0136(02)00101-2)

- Nieslony, P., Cichosz, P., Krolczyk, G.M., Legutko, S., Smyczek, D. & Kolodziej, M. 2016.** Experimental studies of the cutting force and surface morphology of explosively clad Ti-steel plates. *Measurement* **78**:129-137. <https://doi.org/10.1016/j.measurement.2015.10.005>
- Olabi, A.G., Casalino, G., Benyounis, K.Y. & Hashmi, M.S.J. 2006.** An ANN and taguchi algorithms integrated approach to the optimization of CO₂ laser welding. *Advances in Engineering Software* **37**:643-648. <https://doi.org/10.1016/j.advengsoft.2006.02.002>
- Palani. S. & Natarajan, U. 2011.** Prediction of surface roughness in CNC end milling by machine vision system using artificial neural network based on 2D fourier transform. *The International Journal of Advanced Manufacturing Technology* **54**:1033-1042. <https://doi.org/10.1007/s00170-010-3018-3>
- Palavar, O., Özyürek, D. & Kalyon, A. 2015.** Artificial neural network prediction of aging effects on the wear behavior of IN706 superalloy. *Materials & Design* **82**:164-172. <https://doi.org/10.1016/j.matdes.2015.05.055>
- Pourahakbar, H., Khalaj, M., Nazerfakhari, M. & Khalaj, G. 2015.** Artificial neural networks for hardness prediction of HAZ with chemical composition and tensile test of X70 pipeline steels. *Journal of Iron and Steel Research, International* **22**:446-450. [https://doi.org/10.1016/S1006-706X\(15\)30025-X](https://doi.org/10.1016/S1006-706X(15)30025-X)
- Prazmowski, M., Rozumek, D. & Paul, H. 2017.** Static and fatigue tests of bimetal Zr-steel made by explosive welding. *Engineering Failure Analysis* **75**:71-81. <https://doi.org/10.1016/j.engfailanal.2016.12.022>
- Shojaeefard, M.H., Behnagh, R.A., Akbari, M., Givi, M.K.B. & Farhani, F. 2013.** Modelling and pareto optimization of mechanical properties of friction stir welded AA7075/AA5083 butt joints using neural network and particle swarm algorithm. *Materials & Design* **44**:190-198. <https://doi.org/10.1016/j.matdes.2012.07.025>
- Topolski, K., Szulc, Z. & Garbacz, H. 2016.** Microstructure and properties of the Ti6Al4V/Inconel 625 bimetal obtained by explosive joining. *Journal of Materials Engineering and Performance* **25**(8): 3231-3237. <https://doi.org/10.1007/s11665-016-2080-x>
- Wang, B., Xie, F., Luo, X. & Zhou, J. 2016.** Experimental and physical model of the melting zone in the interface of the explosive cladding bar. *Journal of Materials Research and Technology* **5**(4):333-338. <https://doi.org/10.1016/j.jmrt.2016.04.001>
- Xie, M.X., Shang, X.T., Zhang, L.J., Bai, Q.L. & Xu, T.T. 2018.** Interface characteristic of explosive-welded and hot-rolled TA1/X65 bimetallic plate. *Metals* **8**(3):159. <https://doi.org/10.3390/met8030159>